THE JOURNAL OF PHYSICAL CHEMISTRY C
A JOURNAL OF THE AMERICAN CHEMICAL SOCIETY

pubs.acs.org/JPCC

Article

Correlation between Spectroscopic and Mechanical Properties of Gold Nanocrystals under Pressure

Published as part of The Journal of Physical Chemistry virtual special issue "Marie-Paule Pileni Festschrift".

Camino Martín-Sánchez,* Ana Sánchez-Iglesias, Paul Mulvaney, Luis M. Liz-Marzán, and Fernando Rodríguez*

Cite This: *J. Phys. Chem. C* 2022, 126, 1982−1990

Read Online

ACCESS | Metrics & More | Article Recommendations

ABSTRACT: The effects of nonhydrostatic pressure on the morphology and stability of gold nanorods (AuNRs) and nanospheres (AuNSs) in 4:1 methanol−ethanol mixtures were studied by optical absorption spectroscopy and transmission electron microscopy at pressures of up to 23 and 30 GPa, respectively. Solvent solidification and associated nonhydrostatic stresses were found to have a negligible effect on the shape and size of AuNSs. On the contrary, while AuNRs maintained their initial morphology in the hydrostatic range, the uniaxial stress component induced under nonhydrostatic conditions had a shearing effect on the AuNRs, breaking them into smaller particles. Interestingly, colloidal stability was maintained in all cases, and the particles showed no sign of aggregation, despite the severe nonhydrostatic conditions to which both AuNR and AuNS colloids were subjected.

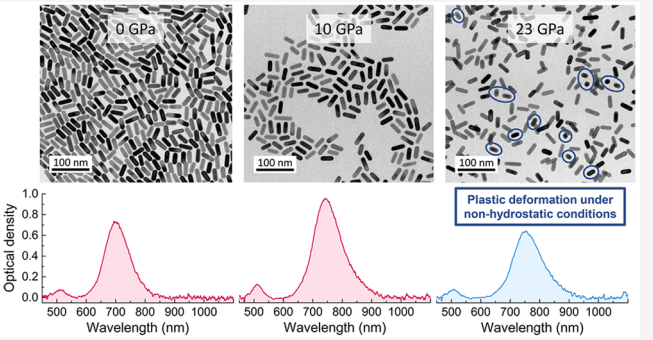

1. INTRODUCTION

The application of hydrostatic pressure provides a promising method for studying the mechanical properties of nanocrystals. Information on the strength, stiffness, and elasticity of the material can be gleaned from measurements of the sample volume as a function of the applied pressure. The volume reduction of both the nanoparticles (NP) and the surrounding medium can be monitored using a range of techniques. Particularly attractive are those methods based on optical spectroscopy, which exploit the high sensitivity of surface plasmonic resonances (SPR) in metal nanoparticles. Although the first measurements of the effect of pressure on the SPR peak position, for several Au and Ag hydrosols, were reported in the early 1990s,[1] interest in studying plasmon-related spectroscopic properties under pressure has skyrocketed during the last 15 years.[2−10] The application of pressure is known to induce SPR shifts as a result of two competing effects.[7] First, the compression of the solvent increases its density, thereby leading to an increase in the solvent refractive index, which in turn causes a red shift in the SPR. Second, the compression of the conduction electrons increases the bulk plasma frequency, which leads to a blue shift.

To generate large hydrostatic pressures, a pressure-transmitting medium (PTM) (typically a liquid or gaseous medium) is employed, with the objective of transforming the uniaxial pressure applied by the diamonds (in a diamond anvil cell, DAC) into hydrostatic pressure. However, at a certain point, the PTM solidifies and the pressure across the cavity becomes inhomogeneous, resulting in the appearance of uniaxial stress components. Under a hydrostatic load, it is assumed that the NPs will compress isotropically, thus retaining their shape under pressure. However, under nonhydrostatic conditions the stresses along the different axes of the nanoparticles differ, inducing changes in the NP morphology. These effects have been directly observed using optical absorption spectroscopy measurements on gold nanorods (AuNRs).[7,8] Earlier reports on gold nanospheres (AuNSs) associated the changes in the extinction spectra at high pressure with pseudoelasticity effects (i.e., oblate deformation under nonhydrostatic conditions).[11] However, no such spectroscopic anomalies have been directly observed in more recent measurements on AuNSs.[10] Whereas the behavior of AuNSs is quite similar in both hydrostatic and nonhydrostatic regimes, AuNRs show abnormal behavior of

Received: December 22, 2021
Revised: January 11, 2022
Published: January 24, 2022

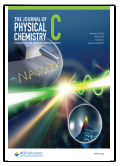

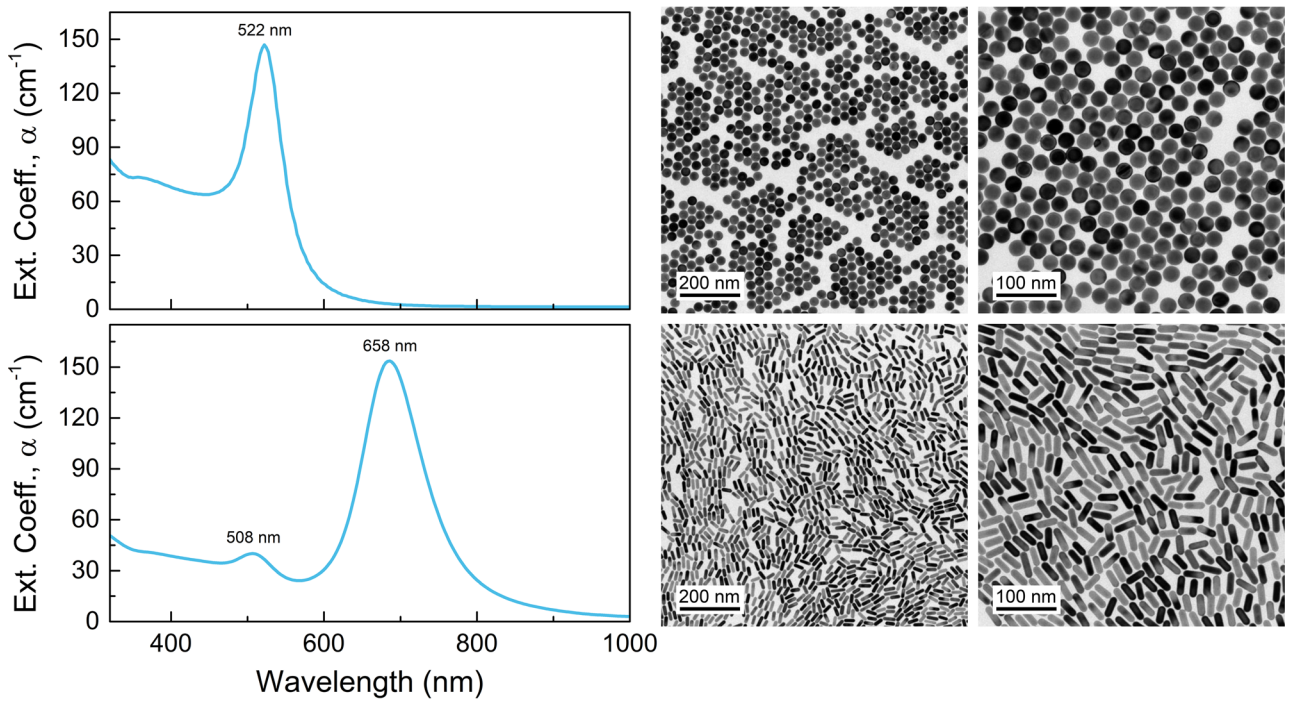

Figure 1. Optical extinction spectra and representative TEM images at different magnifications of the nanoparticles used in the experiments: 28 nm AuNS with [Au] = 12.3 mM (top row) and 34.5 nm × 11.8 nm AuNR with [Au] = 7.0 mM (bottom row).

the surface plasmon resonance and absorption cross-section above the PTM solidification pressure. This anomalous behavior of AuNRs with respect to AuNSs under non-hydrostatic conditions has been attributed to either NP aggregation or NP deformation. However, to the best of our knowledge, there has not been any experimental evidence supporting this hypothesis. Bao et al.[4] reported transmission electron microscopy (TEM) images of 80 nm AuNPs after plastic deformation. They achieved this by loading a water-based AuNP colloid into a DAC and compressing it to form a mixture of AuNPs and ice with applied pressures exceeding 1.2 GPa. Hence, the NPs were not subjected to hydrostatic pressure but experienced anisotropic compression by the surrounding ice. In fact, the reported TEM images showed that NP reshaping was likely due to pressure-induced aggregation and NP sintering rather than the reshaping of individual NPs due to nonhydrostatic effects. The possibility to distinguish reshaping effects from aggregated NPs or individual AuNPs induced under nonhydrostatic conditions is of fundamental importance for an improved understanding of the mechanical properties of AuNPs. In particular, it is critical to determine the pseudoelastic limits yielding permanent plastic deformation in dislocation-free, single-crystal AuNPs.

We present herein a systematic study of the plasmonic response of AuNR and AuNS colloids in methanol−ethanol (MeOH−EtOH) 4:1, in both the hydrostatic and non-hydrostatic regimes, as well as their morphology and stability under high-pressure conditions. We use TEM to explore NP aggregation, deformation, and alloying, after a high-pressure treatment, by recovering the sample after it has been subjected to either hydrostatic or nonhydrostatic pressure of about 30 GPa, with uniaxial stress components in the latter case of up to 2 GPa. We demonstrate that AuNPs remain colloidally stable despite the severely nonhydrostatic conditions and that both NP morphology and crystallinity determine the likelihood that they will undergo permanent plastic deformation.

2. METHODS

2.1. Nanoparticle Synthesis. *2.1.1. Chemicals.* Gold(III) chloride trihydrate ($HAuCl_4$, ≥99%), hexadecyltrimethylammonium bromide (CTAB, ≥99%), sodium borohydride ($NaBH_4$), hexadecyltrimethylammonium chloride (CTAC, 25 wt% in water), benzyldimethylhexadecylammonium chloride (BDAC), ascorbic acid (AA, ≥99%), hydroquinone (HQ, ≥99%), silver nitrate ($AgNO_3$, ≥98%), and *O*-[2-(3-mercaptopropionylamino)ethyl]-*O*′-methylpoly(ethylene glycol) (PEG-SH, M_w = 5K) were purchased from Sigma-Aldrich. Ethanol and methanol were purchased from Scharlab. All chemicals were used without further purification. Milli-Q water (resistivity 18.2 MΩ·cm at 25 °C) was used in all experiments. All glassware was cleaned with aqua regia, rinsed with Milli-Q water, and dried before use.

2.1.2. Synthesis of Single-Crystalline AuNS and AuNR. Single-crystalline AuNS and AuNR were synthesized via well-established seeded-growth methods.[12,13] First, gold seeds (∼1.5 nm) were prepared by the fast reduction of $HAuCl_4$ (5 mL, 0.25 mM) with freshly prepared $NaBH_4$ (0.3 mL, 10 mM) in aqueous CTAB solution (100 mM) under vigorous stirring for 2 min at room temperature and were then kept undisturbed at 27 °C for 30 min to ensure the complete decomposition of sodium borohydride. The mixture changed from light yellow to brownish, indicating the formation of gold seeds. An aliquot of seed solution (0.6 mL) was added under vigorous stirring to a growth solution containing CTAC (100 mL, 100 mM), $HAuCl_4$ (0.36 mL, 50 mM), and ascorbic acid (0.36 mL, 100 mM). The mixture was left undisturbed for 12 h at 25 °C. The solution containing gold nanoparticles (12 nm in diameter) was centrifuged (9000 rpm for 1 h) to remove

https://doi.org/10.1021/acs.jpcc.1c10767
J. Phys. Chem. C 2022, 126, 1982−1990

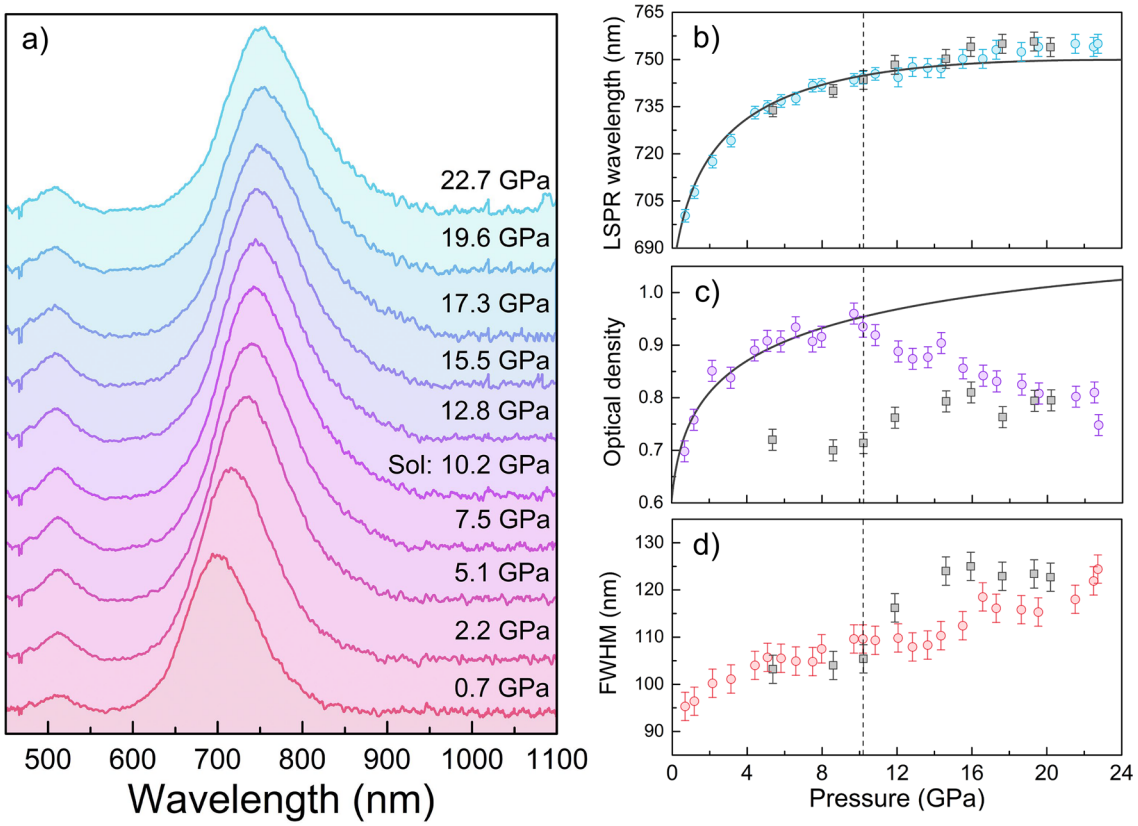

Figure 2. (a) Extinction spectra of AuNRs (AR = 3.0 AuNR in 4:1 MeOH−EtOH) as a function of pressure (raw data). (b) Pressure dependence of the LSPR position of AuNRs. (c) Optical density at the LSPR maximum as a function of applied pressure. (d) Pressure dependence of the fwhm of the LSPR band. Circles and squares correspond to upstroke and downstroke experimental data, respectively. Lines represent the calculated values of $\lambda_{LSPR}(P)$ and the extinction cross-section from Gans theory. Vertical dashed lines indicate the hydrostatic limit of the pressure-transmitting medium.

excess CTAC and ascorbic acid and redispersed in 1 mM CTAB to a final gold concentration of 1 mM.

To grow 12 nm gold nanospheres of up to 28 nm in diameter, an aliquot of 12 nm AuNS solution (2.14 mL, 1 mM) was added under magnetic stirring to a growth solution (100 mL) containing benzyldimethylhexadecylammonium chloride (BDAC, 100 mM), $HAuCl_4$ (0.25 mM), and ascorbic acid (0.5 mM). The mixture was left undisturbed for 30 min at 30 °C and then washed twice by centrifugation (8000 rpm for 1 h). The particles were finally dispersed in 1 mM CTAB to a final gold concentration of 1 mM.

Gold nanorods were synthesized as described elsewhere[13] with minor modifications. An aliquot of gold seeds (~1.5 nm, 1 mL) was added under vigorous stirring to a growth solution containing CTAB (100 mL, 100 mM), $HAuCl_4$ (1 mL, 50 mM), HQ (15 mL, 100 mM), and $AgNO_3$ (1.4 mL, 10 mM). Stirring was stopped after 5 min, and the mixture was then left undisturbed for 2 h at 30 °C. The nanoparticles were washed by two rounds of centrifugation (8000 rpm, 30 min) to remove excess reagents. After the second centrifugation step, the solution was redispersed in CTAB (100 mM) to a final gold concentration of 1 mM. Gold nanorods (15 mL, 1 mM) were partially oxidized with Au^{3+} (3 mL, 1 mM, 1 mL/h) until the longitudinal absorption band was located at 685 nm. Then, the solution was centrifuged (9000 rpm for 1 h) and redispersed in 1 mM CTAB. The concentration of gold for ligand exchange was 1 mM.

2.1.3. Ligand Exchange. [14] To replace the surfactant and transfer the gold nanoparticles to the alcohol mixture, thiolated poly(ethylene glycol) (PEG-SH) with a Dalton molecular weight of 5K was used. An aqueous solution of PEG-SH (10.9 mg for 28 nm gold nanospheres and 21.3 mg for gold nanorods, dissolved in 2 mL of water) was added dropwise under stirring to a dispersion of gold nanoparticles (12 mL, 1 mM) in 1 mM CTAB. The solution was stirred for 2 h and then centrifuged twice in a mixture of methanol−ethanol 4:1. PEGylated gold nanoparticles were finally dispersed in methanol−ethanol 4:1.

Representative TEM images and extinction spectra of the AuNP colloids employed in the experiments are shown in Figure 1. The investigated AuNSs had an average diameter of 27.8 ± 0.6 nm and a characteristic SPR band centered at 522 nm. AuNRs had a mean length of 34.5 ± 1.5 nm, a mean diameter of 11.8 ± 0.6 nm, and an AR distribution of 3.0 ± 0.3, and the optical spectrum showed the characteristic band structure associated with a transversal SPR at 510 nm and a longitudinal SPR (LSPR) at 658 nm.

2.2. High-Pressure Extinction Spectroscopy. High-pressure experiments were carried out in a Boëhler-Almax DAC equipped with ultralow-fluorescence diamond IIa anvils with 350 μm diameter culets. The 200-μm-thick Inconel gaskets were preindented to 40−50 μm and 100-μm-diameter holes were drilled with a BETSA motorized electrical discharge machine to create the hydrostatic chamber. The DAC was loaded with 4:1 MeOH−EtOH AuNP solutions and several

https://doi.org/10.1021/acs.jpcc.1c10767
J. Phys. Chem. C 2022, 126, 1982−1990

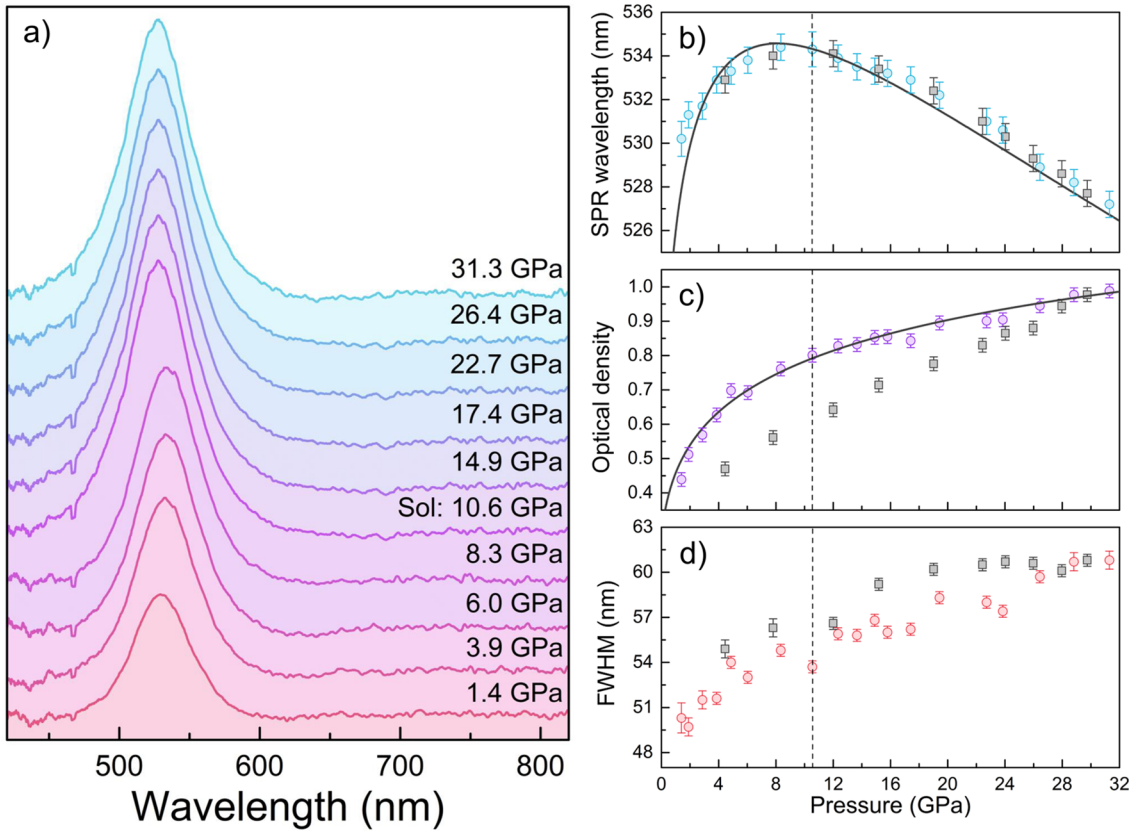

Figure 3. (a) Extinction spectra of 28 nm AuNS in 4:1 MeOH−EtOH as a function of pressure (raw data). (b) Pressure dependence of the SPR position for AuNS. (c) Optical density at the SPR maximum, corrected for sample thickness, as a function of applied pressure (t = 50 μm at ambient pressure). (d) Pressure dependence of the fwhm of the SPR band. Circles and squares correspond to upstroke and downstroke experimental data, respectively. Lines represent the calculated values of $\lambda_{SPR}(P)$ and extinction cross sections from Gans theory. Vertical dashed lines indicate the hydrostatic limit of the pressure-transmitting medium.

ruby microspheres (10−30 μm diameter) as pressure probes.[15] The solution itself acted as the pressure-transmitting medium. The hydrostatic pressure range and liquid−solid pressure transition of AuNP solutions were determined from the pressure dependence of the full width at half-maximum (fwhm) of the ruby emission R lines, whereas the pressure inside the cavity was determined from the R2 line shift following the accepted pressure-dependence protocols established elsewhere.[16]

Optical absorption spectra under high-pressure conditions were collected on a home-built fiber-optic-based microscope[17] equipped with two Cassegrain 20× reflecting objectives mounted on two independent $x-y-z$ translational stages for the microfocus beam, the objective lens, and a third independent $x-y$ translation stage for the DAC holder. Spectra in the UV−visible and near-IR ranges were recorded with two spectrometers: an Ocean Optics USB 2000 and a NIRQUEST 512 employing Si- and InGaAs-CCD detectors, respectively. The I and I_0 transmitted intensities were measured in two separate experiments with the same DAC by loading it first with the AuNP solutions (I) and then with the corresponding solvent (I_0), covering the same pressure range.

2.3. Transmission Electron Microscopy. TEM measurements were performed on a JEM 2100 (JEOL) microscope. AuNP colloids were measured before and after high-pressure treatment. In the latter case, the sample was recovered from the pressure chamber of the gasket by transferring the colloidal mixtures onto copper grids by touching the culet surface of the diamond anvil after pressure release. This method could have accidentally dragged some external nanoparticles from the hydrostatic cavity onto the grid, and these external nanoparticles would not have undergone any pressure treatment. Although sometimes it could be difficult to distinguish which nanoparticles had been under pressure, we assumed that deformed/bent nanoparticles (approximately 1 out of 200, depending on each particular load and nanoparticle morphology) corresponded to compressed particles. Another key parameter in identifying compressed regions was the presence of organic compounds from the partial polymerization of the solvent when subjected to very high pressures. This method allowed us to explore the aggregation state as well as the morphology (size and shape) of the compressed NPs.

3. RESULTS AND DISCUSSION

Variations in the extinction spectra of AuNRs and AuNSs in 4:1 MeOH−EtOH with pressure during both the upstroke and downstroke are shown in Figures 2 and 3, respectively. We interpreted the results in terms of the Gans theory, following the methodology described elsewhere.[7] This analysis allowed us to correlate the pressure-induced SPR shift with relative changes in the AuNP volume−electron density and with the solvent refractive index at each pressure through the following equation

$$\lambda_{SPR} = \lambda_p(0)\sqrt{\frac{V}{V_0}}\sqrt{\varepsilon(0) + \frac{1-L}{L}\varepsilon_m} \quad (1)$$

https://doi.org/10.1021/acs.jpcc.1c10767
J. Phys. Chem. C 2022, 126, 1982−1990

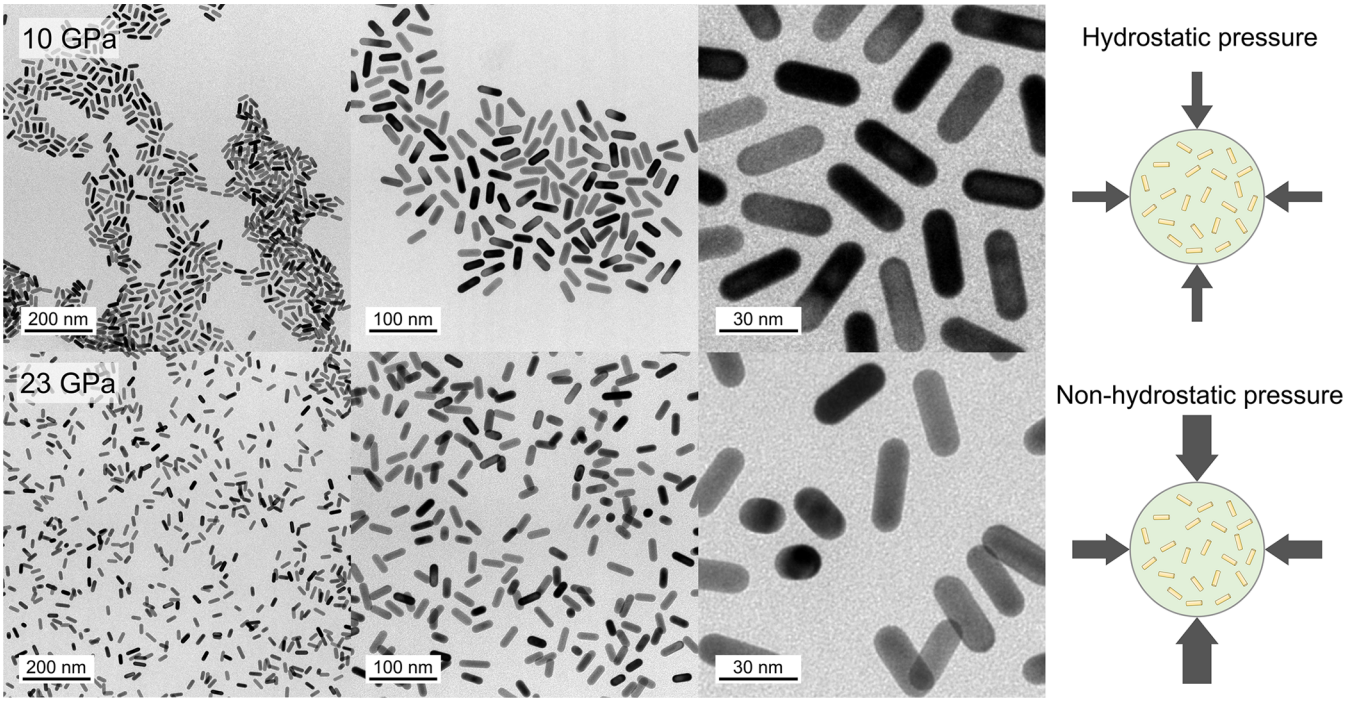

Figure 4. Representative TEM images at different magnifications of AuNR (AR = 3.0) from a 4:1 MeOH−EtOH colloid recovered after being subjected to a pressure of either 10 GPa (top panel) or 23 GPa (bottom panel). A schematic view of the forces acting on the pressure chamber is shown on the right side.

and the optical density at the SPR peak obeys

$$I_{SPR} = \frac{CV\varepsilon_m^{3/2}}{\lambda_{SPR}} \quad (2)$$

Here, $\lambda_p(0)$ and $\varepsilon(0)$ are the plasma wavelength at zero pressure and the high-frequency, short-wavelength dielectric constant of gold, respectively. SPR data (Figures 2 and 3) were analyzed using $\lambda_p(0)$ = 138.5 nm and $\varepsilon(0)$ = 7.9 for nanorods and $\lambda_p(0)$ = 147 nm and $\varepsilon(0)$ = 8.7 for nanospheres. These values provided the overall best fit for each morphology. L is the nanoparticle depolarization or shape factor that was determined from the analysis of the TEM image, ε_m is the dielectric function of the nonabsorbing medium, and C in eq 2 is a renormalization constant. The change in particle volume can be well described by a Vinet equation of state[18]

$$P = 3K_0\frac{1-f}{f^2}\exp\left[\frac{3}{2}(K_0' - 1)(1-f)\right] \quad (3)$$

with $f = (V/V_0)^{1/3}$. We employed a gold bulk modulus of K_0 = 171 GPa with a value of K_0' = 5.72, as determined by the study of the compressibility of gold nanocrystal colloids by X-ray diffraction with synchrotron radiation in the 0−30 GPa range.[19]

It should be noted that a pressure-induced red shift of the LSPR was observed for the AuNR colloid in the hydrostatic range. The variation of $\lambda_{LSPR}(P)$ can be fairly well described through the Gans model in the hydrostatic regime, considering the calibrated refractive index of the 4:1 MeOH−EtOH solvent[10,20] and the equation of state of AuNPs.[19] In the downstroke, the longitudinal resonance blue shifted when the pressure was released. However, it was slightly red-shifted with respect to the upstroke values, more markedly in the nonhydrostatic region (solidified colloid). In addition, the variation of the optical density at the LSPR maximum as a function of pressure showed an abrupt decrease in $I(P)$ above the solution solidification pressure. As expected from model simulations, we observed an increase in the maximum optical density with increasing pressure, mainly due to an increase in the medium refractive index (i.e., density) in the hydrostatic regime (eq 2). Nonetheless, this trend did not hold in the nonhydrostatic pressure range (i.e., after solvent solidification). It is worth noting that the optical density exhibited no reversibility with pressure, showing significant deviations with respect to the initial values when the pressure was removed. The optical density of the downstroke remained almost constant during relaxation. Finally, the LSPR band broadened progressively with pressure, increasing its initial value to up to 30% at 20 GPa. Notwithstanding, broadening was almost reversible with pressure despite entering the nonhydrostatic regime.

Very different behavior was observed for the pressure dependence of the AuNS extinction spectra (Figure 3). The pressure behavior of the AuNS SPR exhibited two clearly differentiated regimes: a rapid red shift with increasing pressure in the 0−7 GPa range followed by a slower blue shift in the higher-pressure range. In the first regime, the increase in the solvent refractive index with pressure is the dominant effect, whereas in the second regime, the increase in the electron density of gold nanospheres becomes more important since the solvent becomes less compressible than gold ($K_{0,sol}' > K_{0,Au}'$). It is important to note that this effect is amplified in the case of spheres since they exhibit a weaker dependence of the SPR to changes in the solvent refractive index than rods do because of their larger depolarization factor: L_{NS} = 1/3, L_{NR} > 1/3, and L_{NR} = 0.978 for AR = 3.[10] Interestingly, the variation of the SPR wavelength with pressure can be well described by Gans theory for both the hydrostatic and nonhydrostatic regimes. In addition, despite the strong nonhydrostatic conditions to which Au nanospheres

https://doi.org/10.1021/acs.jpcc.1c10767
J. Phys. Chem. C 2022, 126, 1982−1990

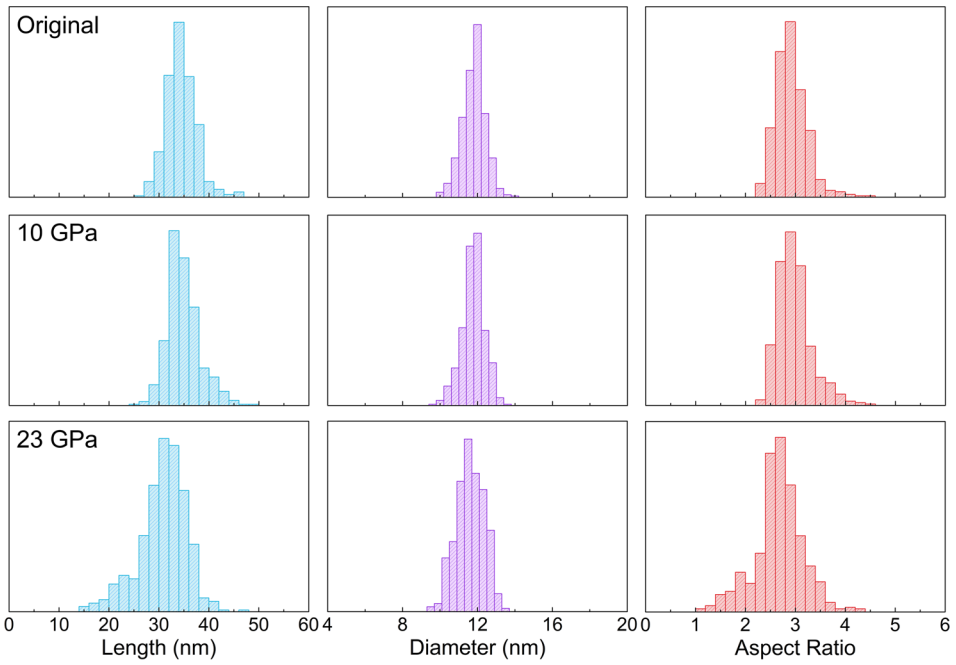

Figure 5. Length, diameter, and aspect ratio distributions determined from TEM images of nonpressurized (top row), pressurized up to 10 GPa (middle row), and pressurized up to 23 GPa (bottom row) AuNRs in 4:1 MeOH−EtOH AR = 3.0 colloids.

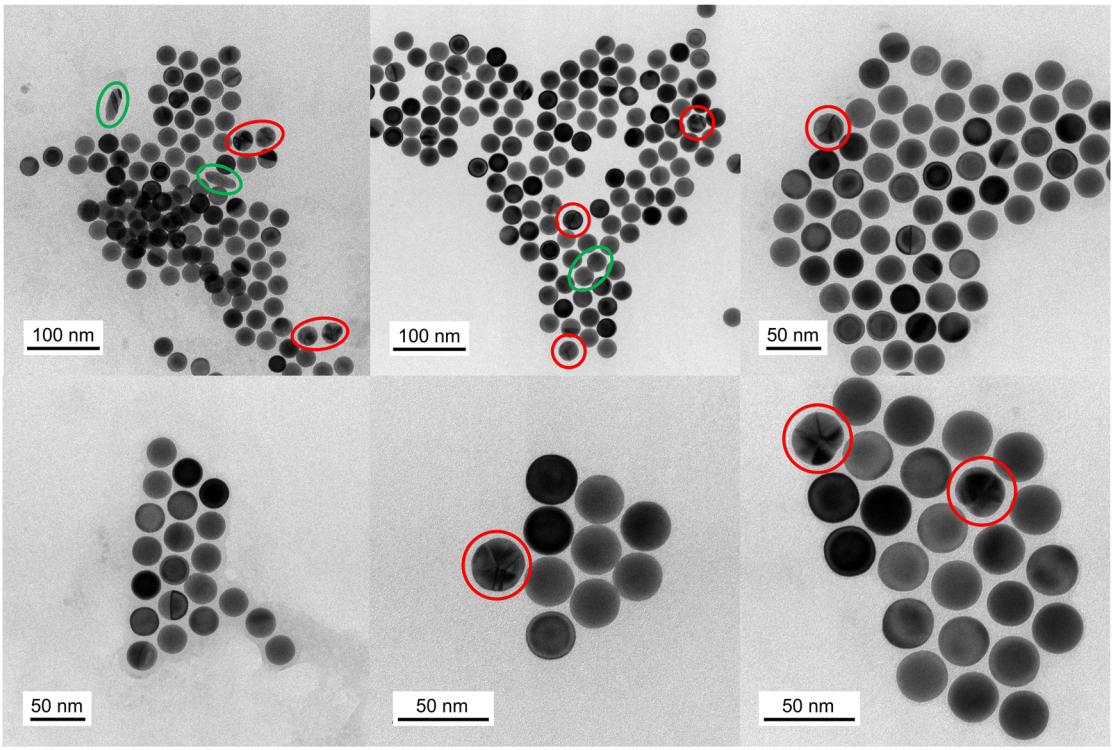

Figure 6. Representative TEM images of the recovered 4:1 MeOH−EtOH AuNS colloid after being subjected to a high-pressure treatment of 31 GPa. Red and green circles surround nanospheres that have suffered slight surface deformations and more important deformation/sintering effects, respectively.

were subjected (axial stress component of σ = 1 at 20 GPa[19]), the SPR wavelength was found to be completely reversible, within measurement uncertainty, in the downstroke. Furthermore, we observed a continuous increase in the optical density at the SPR maximum with increasing pressure. Neither the SPR position nor the optical density underwent any significant change associated with colloid solidification, as was observed in AuNR colloids. In the downstroke, the optical density at the SPR progressively decreased with decreasing pressure but had slightly smaller values with respect to the upstroke values. Finally, we observed a weaker dependence with pressure of the fwhm of the SPR band in AuNSs than in AuNRs, with an increase of 20% over 30 GPa.

https://doi.org/10.1021/acs.jpcc.1c10767
J. Phys. Chem. C 2022, 126, 1982−1990

Figure 4 shows representative TEM images of AuNR from a dispersion in 4:1 MeOH−EtOH, recovered after pressure treatment at either 10 GPa (pure hydrostatic conditions) or 23 GPa (both hydrostatic and nonhydrostatic regimes). Shown in Figure 5 are histograms of the length, diameter, and aspect ratio distributions for nanorods under ambient conditions after applying a hydrostatic pressure of 10 GPa and under nonhydrostatic conditions for up to 23 GPa. Initially, the AuNRs had a mean length of l = 34.5 ± 1.5 nm, a mean diameter of d = 11.8 ± 0.6 nm, and a mean aspect ratio of AR = 3.0 ± 0.3. After exposure to hydrostatic pressure at 10 GPa, the AuNR size distribution was found to be identical, within experimental uncertainty (l = 34.9 ± 1.6 nm, d = 11.8 ± 0.6 nm, and AR = 3.0 ± 0.3), revealing that, in agreement with optical absorption spectroscopy, no gold nanorod is plastically deformed when compressed under hydrostatic pressure conditions.

However, TEM images of the recovered AuNRs after a pressure treatment of up to 23 GPa revealed the presence of smaller aspect ratio nanorods (AR = 1 to 2), which were not observed in the starting colloid. Furthermore, the size distributions (Figure 5) revealed that the smaller aspect ratio nanorods were generated through a reduction in rod length but the mean diameter of the analyzed nanorods remained constant: l = 31 ± 3 nm, d = 11.7 ± 0.7 nm, and AR = 2.7 ± 0.5. These data indicate that the uniaxial stresses derived from the solidification of the solvent had a shear effect on the nanorods, breaking them into smaller fragments/particles. From the size and shape distributions, we estimate that the number of AuNRs which underwent plastic deformation was about 40% and that the remaining 60% retained the same size and shape as in the initial (noncompressed) colloid. This resulted in a marked broadening of the length and aspect ratio distributions as well as a decrease in their mean values. Surprisingly, we did not observe any evidence of nanoparticle aggregation. An exception to this behavior is given by a small number of nanorods that appeared to be "piled up", likely as a result of the drying process on the grid. However, most nanorods maintained a distance that was consistent with the presence of PEG on their surface, thus confirming its suitability as a nanoparticle stabilizing agent, even under nonhydrostatic pressure conditions.

Figure 6 shows representative TEM images of 28 nm AuNS from a 4:1 MeOH−EtOH colloid, recovered after a pressure treatment of up to 31 GPa (both hydrostatic 0−10 GPa and nonhydrostatic 10−31 GPa regimes). The initial spheres had a mean diameter of 27.8 ± 0.6 nm. After the pressure treatment, the size distribution was found to be 27.7 ± 0.7 nm in diameter. According to this result, we can conclude that there is neither significant permanent plastic deformation nor an increase in the size distribution of the nanoparticles. The AuNS original average dimensions were maintained despite having been subjected to severe nonhydrostatic conditions. Interestingly, single-crystal spheres are found to be extremely stable under nonhydrostatic pressure. In contrast, polycrystalline AuNSs (those initially containing twin planes) undergo slight surface deformation while retaining a spherical shape. On the other hand, TEM images also reveal that some ellipsoidally shaped nanoparticles are also present after compression. However, these deformed nanoparticles represent a small fraction of 1 in 300 deformed AuNPs. TEM images reveal that most of the particles maintain interparticle distances compatible with the presence of the stabilizing agent, as already noted for AuNR colloids. It must be noted that, although the PEG molecular weight would yield larger interparticle distances, when the NP colloid drop dries on the grid for TEM observation, PEG chains collapse whereas in solution they are expanded. Therefore, the final distance between nanoparticles is reduced after drying.

Given that the nonhydrostatic axial stress component at 31 GPa is known to be $\sigma \approx 2$ GPa from XRD,[19] we conclude that the critical shear stress should be about this value. Note that the fraction of nanospheres undergoing plastic deformation is much smaller than that of broken nanorods at 20 GPa, thus indicating that the nanorods are shear cut along the longitudinal direction of the nanorod. The critical stress for nanorod breakage is thus smaller than the critical shear stress for spheres, probably because of the larger area for deformation in spheres as compared to that in nanorods. The nanorod diameter is 12 nm, and the nanosphere diameter is 28 nm. Additionally, the spherical shape is expected to be more stable than the anisotropic nanorods against axial stress.

Our pressure experiments provide direct evidence of the differences in the behavior of gold rods and spheres under nonhydrostatic loads. The anomalous effects observed in the extinction spectrum under nonhydrostatic pressure conditions[7,8,21] are likely due to the fracture of nanorods because of axial stresses generated by the solidified solvent, ruling out an aggregation process. These TEM results have different implications for the variation of the AuNR extinction spectra with pressure. First, after AuNR fracture induced by nonhydrostatic uniaxial stress components takes place, a fraction of AuNRs do not contribute to the LSPR maximum but their signal spreads out over a spectral range mainly determined by their length and AR. This effect produces an abrupt decrease in optical density above the solidification pressure. Given that this fraction of broken AuNRs increases with applied pressure, the optical density should decrease gradually with pressure, as can be seen in Figure 2c. The LSPR of the fragmented AuNRs is shifted according to their aspect ratio, so their contribution to the optical density at the LPSR maximum is smaller than that for nonfragmented AuNRs. The optical density reduction is consistent with 40% of fragmented AuNRs considering that nonfragmented AuNRs have a full contribution at the LSPR maximum, whereas fragmented AuNRs have a partial contribution depending on the AuNR fragmentation structure. In addition, the extinction cross-section σ_{ext} is proportional to the AuNR AR,[22] and when the average AR is reduced, so is the associated σ_{ext}. On the contrary, although nonhydrostatic pressure produces a reduction in the average AuNR aspect ratio, a slight red shift was observed in the LSPR wavelength above the solidification pressure. It has been observed experimentally that the AuNR LSPR wavelength above the solidification pressure shifts, depending on the solvent, to either longer or shorter wavelengths with respect to the LSPR under purely hydrostatic conditions.[7,21] This suggests that, despite having a lower AR after solidification, the overall LSPR of the AuNR can either red shift or blue shift depending on the solvent solidification. The presence of nearby AuNR induced by solvent solidification may be a possible explanation for the unexpected slight LSPR red shift observed in the 4:1 MeOH−EtOH AuNR colloid. After partial AuNR fragmentation, AuNRs remaining isolated would generate a blue shift while those forming clusters would generate a red shift. Both effects would induce either LSPR red shifts or blue shifts with pressure in the nonhydrostatic regime, depending on which is

https://doi.org/10.1021/acs.jpcc.1c10767
J. Phys. Chem. C 2022, 126, 1982−1990

the dominant effect. Nonetheless, this hypothesis deserves further experimental verification by specific techniques allowing in situ direct observations in a DAC.

The progressive increase in the fwhm with pressure is slightly more pronounced in the nonhydrostatic region, which is likely related to broadening of the aspect ratio distribution in the colloid. However, this increase is not drastic since the lower-AR AuNRs do not strongly affect the overall fwhm of the LSPR band. In view of these results, the optical density appears to be the parameter that is the most sensitive to morphological changes undergone by AuNR under nonhydrostatic conditions. Both the fwhm and the LSPR wavelength are less sensitive to AuNR plastic deformations, so they do not constitute a consistent spectroscopic sensor of the effects of nonhydrostaticity in AuNR colloids.

Interestingly, the broken AuNRs have rounded ends and an anisotropic shape. This is in contrast with the expected behavior of AuNRs above the critical shear stress yielding sharp edges, as observed in macroscopic gold rods. The observed reshaping of AuNR yielding rounded tips is likely caused by the high surface energy involved at the nanoscale to retain abrupt shapes. Because AuNRs remain under high-pressure conditions during the downstroke, the pressure itself may favor the softening of the rod ends. Another point of interest concerns the critical shear stress for plastic deformation. The measured axial stress in these AuNR colloids (Figure 4) is just $\sigma = 0$ at 10 GPa and $\sigma = 1$ at 20 GPa, as derived from XRD elsewhere.[19] Whereas at 10 GPa (hydrostatic conditions) we see no AuNR breakage, at 23 GPa 40% of the AuNRs break into smaller nanoparticles, thus indicating that the critical shear stress is lower, about $\sigma_{css} = 1$ GPa. This result is consistent with measurements of the critical shear stress values obtained for gold as a function of particle size, reported elsewhere.[23] Values of $\sigma_{css} = 200$ MPa for a size of 7450 nm and $\sigma_{css} = 500$ MPa for a size of 400 nm were reported therein. Our results confirm this trend with a value of $\sigma_{css} \approx 1$ GPa for AuNRs of $d = 11.8$ nm and AR = 3.0.

TEM images of AuNSs are consistent with the extinction optical spectroscopy measurements carried out in both the upstroke and downstroke. The SPR wavelength, which is determined by the nanoparticle size under the same solvent conditions, is perfectly reversible since the nanoparticles maintain their stability within the colloid and their size of 27.8 ± 0.6 nm (initial dimensions) versus 27.7 ± 0.7 nm (final dimensions), despite the severe nonhydrostatic conditions. Accordingly, there is no significant increase in the polydispersity of the sample after pressure treatment, which accounts for the progressive increase in the resonance fwhm with pressure. Nevertheless, as pressure increases, the medium refractive index (i.e., dielectric constant) also increases. The extinction cross-section associated with a single 28 nm AuNS varies in fwhm by up to 10% when immersed in a medium with a dielectric constant of $\varepsilon_m = 1.76$ with respect to one with $\varepsilon_m = 2.94$,[24,25] corresponding to ε_m values of the 4:1 MeOH−EtOH solvent at ambient pressure and at 31 GPa, respectively.[10,20] This pressure-induced variation in the resonance fwhm is mainly caused by the increase in ε_m itself, which is further intensified by the polydispersity of the sample. This effect is likely responsible for the observed pressure dependence of the fwhm and also explains why fwhm(P) is reversible upon pressure release. Finally, the hysteresis observed in the optical density is related to the plastic deformation of the gasket forming the pressure chamber. In this way, the thickness variations during the downstroke and upstroke are different. This effect yields changes in the effective nanoparticle concentration, causing the optical density to undergo different pressure dependences in both upstroke and downstroke. Nevertheless, both the SPR wavelength and fwhm are completely reversible since these properties are not dependent on the optical path length or the nanoparticle concentration.

4. CONCLUSIONS

We have demonstrated that the abnormal behavior observed in the AuNR extinction spectra under nonhydrostatic high-pressure conditions is due to the partial breakage of gold nanorods induced by a uniaxial stress component of 1 GPa attained in the solidified PTM at 20 GPa. Among the three analyzed spectral parameters—LSPR wavelength, fwhm, and optical density at the LSPR maximum—the optical density is the most sensitive one to the morphological changes in AuNR under nonhydrostatic high-pressure conditions. On the contrary, AuNSs retain their shape and original average dimensions despite being subjected to severely nonhydrostatic conditions at 31 GPa with an axial component of 2 GPa. Interestingly, while single-crystalline AuNSs are extremely stable under nonhydrostatic pressure, polycrystalline nanospheres experience slight superficial plastic deformation. Furthermore, despite the strong nonhydrostatic conditions to which both AuNR and AuNS are subjected (uniaxial stress components of up to 2 GPa), the nanoparticles maintain their colloidal stability without any evidence of aggregation, thus revealing PEG to be an excellent stabilizing agent even under nonhydrostatic pressure conditions.

A remarkable conclusion is that AuNSs constitute a suitable high-pressure plasmonic sensor since they are extremely stable even under severe nonhydrostatic conditions. Conversely, although AuNRs exhibit better spectral sensitivity, their use as high-pressure sensors is restricted to hydrostatic conditions because nonhydrostatic conditions lead to partial nanorod breakage.

AUTHOR INFORMATION

Corresponding Authors

Camino Martín-Sánchez − *MALTA Consolider, DCITIMAC, Facultad de Ciencias, University of Cantabria, Santander 39005, Spain;* orcid.org/0000-0003-3574-7748; Email: martinsc@unican.es

Fernando Rodríguez − *MALTA Consolider, DCITIMAC, Facultad de Ciencias, University of Cantabria, Santander 39005, Spain;* orcid.org/0000-0002-7237-7443; Email: rodriguf@unican.es

Authors

Ana Sánchez-Iglesias − *CIC biomaGUNE, Basque Research and Technology Alliance (BRTA), Donostia-San Sebastián 20014, Spain; Centro de Investigación Biomédica en Red, Bioingeniería, Biomateriales y Nanomedicina (CIBER-BBN), Donostia-San Sebastián 20014, Spain;* orcid.org/0000-0003-1871-8742

Paul Mulvaney − *ARC Centre of Excellence in Exciton Science, School of Chemistry, University of Melbourne, Parkville, Victoria 3010, Australia;* orcid.org/0000-0002-8007-3247

Luis M. Liz-Marzán − *CIC biomaGUNE, Basque Research and Technology Alliance (BRTA), Donostia-San Sebastián 20014, Spain; Centro de Investigación Biomédica en Red,*

https://doi.org/10.1021/acs.jpcc.1c10767
J. Phys. Chem. C 2022, 126, 1982−1990

Bioingeniería, Biomateriales y Nanomedicina (CIBER-BBN), Donostia-San Sebastián 20014, Spain; Ikerbasque, Basque Foundation for Science, Bilbao 48009, Spain; orcid.org/0000-0002-6647-1353

Complete contact information is available at: https://pubs.acs.org/10.1021/acs.jpcc.1c10767

Author Contributions

C.M.-.S. and F.R.: conceptualization and design; C.M.-.S. and F.R.: coordination; C.M.-.S., A.S.-I., L.M.L.-M., and F.R.: investigation and formal analysis; C.M.-.S. and F.R.: original draft; C.M.-.S., A.S.-I., P.M., L.M.L.-M., and F.R.: review and editing; F.R., L.M.L.-M., and P.M.: funding acquisition.

Notes

The authors declare no competing financial interest.

■ ACKNOWLEDGMENTS

Financial support from Projects PGC2018-101464−B-I00 (Ministerio de Ciencia, Innovación y Universidades) and MALTA-Consolider Team (RED2018-102612-T) is acknowledged. We acknowledge J. A. Barreda-Argüeso and J. Ruiz-Fuertes for support with high-pressure measurements. P.M. thanks the ARC for grant CE170100026. L.M.L.-M. acknowledges grant PID2020-117779R and the Maria de Maeztu Units of Excellence Program (grant MDM-2017-0720) from the Spanish Ministerio de Ciencia e Innovación.

■ ABBREVIATIONS

AuNR, gold nanorod; AuNS, gold nanosphere; DAC, diamond anvil cell; fwhm, full width at half-maximum; LSPR, longitudinal surface plasmon resonance; MeOH−EtOH, methanol−ethanol; NP, nanoparticle; PTM, pressure-transmitting medium; SPR, surface plasmon resonance; TEM, transmission electron microscopy

■ REFERENCES

(1) Coffer, J. L.; Shapley, J. R.; Drickamer, H. G. The Effect of Pressure on the Surface Plasmon Absorption Spectra of Colloidal Gold and Silver Particles. *J. Am. Chem. Soc.* **1990**, *112*, 3736−3742.

(2) Christofilos, D.; Assimopoulo, S.; Fatti, N. D.; Voisin, C.; Vallee, V.; Kourouklis, G. A.; Ves, S. High Pressure Study of the Surface Plasmon Resonance in Ag Nanoparticles. *High Pressure Res.* **2003**, *23*, 23−27.

(3) Bao, Y.; Zhao, B.; Hou, D.; Liu, J.; Wang, F.; Wang, X.; Cui, T. The Redshift of Surface Plasmon Resonance of Colloidal Gold Nanoparticles Induced by Pressure with Diamond Anvil Cell. *J. Appl. Phys.* **2014**, *115*, 223503.

(4) Bao, Y.; Zhao, B.; Tang, X.; Hou, D.; Cai, J.; Tang, S.; Liu, J.; Wang, F.; Cui, T. Tuning Surface Plasmon Resonance by the Plastic Deformation of Au Nanoparticles Within a Diamond Anvil Cell. *Appl. Phys. Lett.* **2015**, *107*, 201909.

(5) Gu, X. W.; Hanson, L. A.; Eisler, C. N.; Koc, M. A.; Alivisatos, A. P. Pseudoelasticity at Large Strains in Au Nanocrystals. *Phys. Rev. Lett.* **2018**, *121*, 056102.

(6) Medeghini, F.; Hettich, M.; Rouxel, R. R.; Santos, S. D. S.; Hermelin, S.; Pertreux, E.; Dias, A. T.; Legrand, F.; Maioli, P.; Crut, A.; et al. High-Pressure Effect on the Optical Extinction of a Single Gold Nanoparticle. *ACS Nano* **2018**, *12*, 10310−10316.

(7) Martin-Sanchez, C.; Barreda-Argüeso, J. A.; Seibt, S.; Mulvaney, P.; Rodríguez, F. Effects of Hydrostatic Pressure on the Surface Plasmon Resonance of Gold Nanocrystals. *ACS Nano* **2019**, *13*, 498−504.

(8) Martín-Sánchez, C.; González-Rubio, G.; Mulvaney, P.; Guerrero-Martínez, A.; Liz-Marzaín, L. M.; Rodríguez, F. Monodisperse Gold Nanorods for High-Pressure Refractive Index Sensing. *J. Phys. Chem. Lett.* **2019**, *10*, 1587−1593.

(9) Runowski, M.; Sobczak, S.; Marciniak, J.; Bukalska, I.; Lis, S.; Katrusiak, A. Gold Nanorods as a High-Pressure Sensor of Phase Transitions and Refractive-Index Gauge. *Nanoscale* **2019**, *11*, 8718−8726.

(10) Martin-Sanchez, C.; Sanchez-Iglesias, A.; Mulvaney, P.; Liz-Marzan, L. M.; Rodriguez, F. Plasmonic Sensing of Refractive Index and Density in Methanol−Ethanol Mixtures at High Pressure. *J. Phys. Chem. C* **2020**, *124*, 8978−8983.

(11) Gu, X. W.; Hanson, L. A.; Eisler, C. N.; Koc, A. M.; Alivisatos, A. Pseudoelasticity at Large Strains in Au Nanocrystals. *Phys. Rev. Lett.* **2018**, *121*, 056102.

(12) Zheng, Y.; Zhong, X.; Li, Z.; Xia, Y. Successive, Seed-Mediated Growth for the Synthesis of Single-Crystal Gold Nanospheres with Uniform Diameters Controlled in the Range of 5−150 nm. *Part. Part. Syst. Charact* **2014**, *31*, 266−273.

(13) Vigderman, L.; Zubarev, E. R. High-Yield Synthesis of Gold Nanorods with Longitudinal SPR Peak Greater than 1200 nm Using Hydroquinone as a Reducing Agent. *Chem. Mater.* **2013**, *25*, 1450−1457.

(14) Fernández-López, C.; Mateo-Mateo, C.; Álvarez-Puebla, R. A.; Pérez-Juste, J.; Pastoriza-Santos, I.; Liz-Marzán, L. M. Highly Controlled Silica Coating of PEG-Capped Metal Nanoparticles and Preparation of SERS-Encoded Particles. *Langmuir* **2009**, *25*, 13894−13899.

(15) Syassen, K. Ruby Under Pressure. *High Pressure Res.* **2008**, *28*, 75−126.

(16) Shen, G.; Wang, Y.; Dewaele, A.; Wu, C.; Fratanduono, D. E.; Eggert, J.; Klotz, S.; Dziubek, K. F.; Loubeyre, P.; Fat'yanov, O. V.; Asimow, P. D.; Mashimo, T.; Wentzcovitch, R. M. M.; et al. Toward an International Practical Pressure Scale: A Proposal for an IPPS Ruby Gauge (IPPS-Ruby2020). *High Press. Res.* **2020**, *40*, 299−314.

(17) Barreda-Argüeso, J. A.; Rodríguez, F. Patent No. 2014/000049, 2013.

(18) Vinet, P.; Ferrante, J.; Smith, J. R.; Rose, J. H. A Universal Equation of State for Solids. *J. Phys. C: Solid State Phys.* **1986**, *19*, L467.

(19) Martín-Sánchez, C.; Sánchez-Iglesias, A.; Barreda-Argüeso, J. A.; Polian, A.; Itié, J. P.; Pérez, J.; Mulvaney, P.; Liz-Marzán, L. M.; Rodríguez, F. On the Stiffness of Gold at the Nanoscale. *ACS Nano* **2021**, *15*, 19128−19137.

(20) Eggert, J. H.; Xu, L. W.; Che, R. Z.; Chen, L. C.; Wang, J. F. High Pressure Refractive Index Measurements of 4:1 Methanol:Ethanol. *J. Appl. Phys.* **1992**, *72*, 2453.

(21) Martín-Sánchez, C.; Seibt, S.; Barreda-Argüeso, J. A.; Rodríguez, F. Exploring Pressure Effects on Metallic Nanoparticles and Surrounding Media through Plasmonic Sensing. *J. Phys. Conf. Ser.* **2020**, *1609*, 012009.

(22) Prescott, S. W.; Mulvaney, P. Gold Nanorod Extinction Spectra. *J. Appl. Phys.* **2006**, *99*, 123504.

(23) Greer, J. R.; Oliver, W. C.; Nix, W. D. Size Dependence of Mechanical Properties of Gold at the Micron Scale in the Absence of Strain Gradients. *Acta Mater.* **2005**, *53*, 1821−1830.

(24) Yu, R.; Liz-Marzán, L. M.; García de Abajo, F. J. Universal Analytical Modeling of Plasmonic Nanoparticles. *Chem. Soc. Rev.* **2017**, *46*, 6710−6724.

(25) *Nanophotonics*. Available online: http://www.nanophotonics.es/widgets, accessed Sept 20, 2021.